Journal of Energy Storage 65 (2023) 107364

Contents lists available at ScienceDirect

Journal of Energy Storage

journal homepage: www.elsevier.com/locate/est

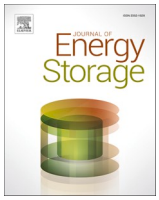

Research papers

A new concept of highways infrastructure integrating energy storage devices for e-mobility transition

D. Pelosi [a], M. Longo [b], G. Bidini [a], D. Zaninelli [b], L. Barelli [a,*]

[a] Department of Engineering, University of Perugia, Via G. Duranti 1/A4, 06125 Perugia, Italy
[b] Department of Energy, Politecnico di Milano, Via La Masa 34, 20156 Milano, Italy

ARTICLE INFO

Keywords:
Electric and hydrogen mobility
Electrolyzer
Energy storage
Fast charging station
Hydrogen
Li-ion battery
Vanadium redox flow battery

ABSTRACT

European Commission aims to reach net zero carbon emissions by 2050. Since transport produces 23 % of the global emissions, a massive electrification is necessary. A proper infrastructure for battery and fuel cell electric vehicles (BEVs/FCEVs) charging/refueling should be developed, especially along the highways. This research study illustrates three different alternatives of energy storage integration into fast charging stations (FCSs) aiming to support BEVs/FCEVs fast charging/refueling by exploiting the surplus of renewable energy assessed in Italy at 2040. Specifically, the integration of Lithium-Ion Battery (LIB), Vanadium Redox Flow Battery (VRFB) and LIB/Proton Exchange Membrane Electrolyzer (PEM-E) into FCS is analyzed assessing the overgeneration exploitation and volumetric encumbrance of storage section. Dynamic FCS models are developed for each scenario and simulations are performed to proper sizing the storage components. The paper outcomes highlight that the number of charged/refueled EVs at parity of occupied volume is for the PEM-E case of one order magnitude lower than LIB case. If the comparison is made over the charged/refueled kWh per cube meter, the difference between PEM-E and LIB is significantly reduced (i.e., 11.7 vs. 28 kWh m^{-3}). It is highlighted as BEVs fast charging (once LIB is considered) allows more than halve volume occupation with respect to FCEVs refueling with H_2 on-site production, since territory occupation is a constraint at systemic level. Moreover, the LIB integration allows a reduction up to 53 % of the power requested from the grid with respect to the storage absence, reducing under voltage and power stability issues as well.

1. Introduction

Because of climate change due to greenhouse gases and pollution, the world is facing a great environmental challenge in order to limit the global average temperature below 2 °C at 2100 [1]. In this context, European Commission has presented the long-term EU strategy, to reach net zero carbon emissions by 2050 [2]. To this aim, Europe is moving towards a more sustainable circular economy and decarbonized transport system [3]. As matter of fact, carbon dioxide emissions produced by the transport sector results to be equal to 23 % of the global emissions by sector. Although increasing the efficiency of internal combustion engines cannot drastically yield to a sufficient CO_2 reduction imposed by EU long-term goals, alternative mobilities, such as those based on electricity and hydrogen, are needed. Electric and hydrogen mobilities are considered clean technologies, especially when electricity and hydrogen are generated by renewable energy sources [4–6]. However, current electricity and hydrogen production are almost entirely powered by fossil fuels, with respectively about 28 % and only 4 % of energy coming from renewables [7,8]. Anyway, the decarbonization process imposed by the European Commission will lead to at least 40 GW of renewable hydrogen electrolyzers (i.e., up to 10 million tons of renewable hydrogen in Europe by 2030) and to over 500 GW of installed renewable power to reach a share of *renewables* in the power mix beyond *65* % by 2030 [9,10]. As regards to the advantages of hydrogen has over battery-powered cars and trucks is the speed of refueling, which is the same as for petrol-powered vehicles, as is the range. As matter of fact, mass adoption of battery electric vehicles (BEVs) faces major obstacles due to consumer worries over several important battery-related issues, such as limited range that causes range anxiety, long charging time, lack of charging stations, and high initial cost [11].

Therefore, to overcome such issues, a strong fast charging and hydrogen refueling infrastructure needs to be developed to ensure the deployment of BEVs and fuel cell electric vehicles (FCEVs), aiming to spread electric and hydrogen mobilities as widely as possible. As evident

* Corresponding author.
E-mail address: linda.barelli@unipg.it (L. Barelli).

https://doi.org/10.1016/j.est.2023.107364
Received 10 November 2022; Received in revised form 19 March 2023; Accepted 4 April 2023
Available online 14 April 2023

from Fig. 1a, the fast-charging infrastructure is not yet implemented in the continental Europe, although Germany, Netherlands and Belgium have a wider developed one with respect to Italy, France, and Spain. Specifically, blue points represent fast-charging stations and green lines highlight the gap mileage between two subsequent FCSs which is below 60 km. As regards hydrogen refueling stations, Fig. 1b underlines that only a few points are present in the middle of Europe, almost sited in Germany. Concerning the Italian scenario, only one highway hydrogen refueling station, distributing green hydrogen, is placed along "Brennero" highway [12]. Therefore, the development of an infrastructure for hydrogen refueling in Europe is necessary to boost FCEVs and other hydrogen-based transport means.

Moreover, since the high connection power required is not available everywhere, it often has to be retrofitted at a high cost. An interesting alternative for infrastructures development is the use of batteries as energy storage and proton exchange membrane electrolyzer (PEM-E) for green hydrogen production, which provide a solution to overcome the relating issues of electricity and hydrogen generation from renewables. Several works deal with the fast charging and hydrogen infrastructure for mobility, applying algorithms for the optimal locations of charging stations along the roads, evaluating the investment costs related to such solution and highlighting the main issues to overcome [14–19]. Nevertheless, at the best of our knowledge, no research activity is carried out assessing energy storage and hydrogen generation devices, in terms of encumbrances, to analyze the volumetric impact into a fast-charging station (FCS). Therefore, the aim of this work is to compare, in terms of encumbrances per charged/refueled vehicle, different storage and hydrogen alternatives to be integrated into FCSs installed on highways, to allow:

i) vehicles fast charging and hydrogen refueling in the framework of the expected increase in BEVs and FCEVs spread during the next years.
ii) the exploitation of a part of the renewable overgeneration (OG) assessed for 2040 at national level for BEVs fast charging and hydrogen refueling.

Specifically, the three considered alternatives for FCS are: *i)* Lithium-ion battery (LIB), *ii)* Vanadium Redox Flow Battery (VRFB) and *iii)* LIB and PEM-E stack. The paper is organized as follows: Section 2 describes the implemented methodology, moving from the statistical analysis of OG data to be considered as input to dynamic modeling, definition of the investigated scenarios and proper sizing of the LIBs, VRFBs and PEM-E. Section 3 illustrates the main results obtained from simulations for all the studied scenarios. A comparison among the encumbrances of the alternatives to be integrated into FCS is performed in Section 4. The main outcomes of this research work are detailed in Section 5.

2. Methodology

This section illustrates the procedure implemented for the definition of the components sizing and simulation scenarios.

2.1. Input data and statistical analysis

Since renewable energy sources present a great intermittent and fluctuating behavior, the forecasted boost in renewable power plants will cause a significant mismatch between power demand and generation in the next years. Thus, to perform this analysis, the Italian renewable OG "Scenari 2019" forecasted by TERNA S.p.A. at 2040 is considered.

As input data for the statistical analysis presented below, the OG profile from renewables, and the annual FCS load are implemented. The average and maximum OG power values correspond to about 1.28 GW and 22 GW, respectively. Regarding the recharging infrastructure, ASPI plans 67 highways stations including columns (each one with an installed power of 350 kW) in number from four to six per station in Italy [20]. Thus, per each FCS, five charging columns are assumed resulting in a total installed power of 1.75 MW. For what concerns the FCS load, a typical weekly trend of the 1.75 MW FCS load, depicted in Fig. 2, is implemented with respect to the normalized profile shown in [21]. Subsequently, such load is repeated for an entire year.

Under the assumption of exploiting the available OG for BEVs charging and distributed green hydrogen production, through a proper energy storage system and PEM-E installed at each FCS, a new concept of FCS is presented. Specifically, integrating storage and electrolyzers into the FCS allows the postponed use of renewable OG, contributing to increase the renewable electricity exploitation.

To this aim, a proper statistical analysis is performed. In detail, the statistical distribution of the mean, over a weekly period, of the OG daily hours, is assessed. First, the annual OG power data are grouped week by week (since the FCS load is defined over a week period [21]) and then day by day, assessing how long such profile is not null. Subsequently, the daily OG average value in terms of hours is determined for each week. Second, 25 hourly classes were defined starting from 0, that corresponds to the weeks with null overgeneration, to 24 (i.e., the theoretical case of weeks with OG never null). Thus, classifying the weeks according to such criterion, the occurrences frequency during the year is determined. Moreover, the inverse cumulative probability is calculated to define the value of the OG mean hours for the sizing procedure (as detailed in Section 2.3) performed in MATLAB®/Simulink environment. According to the results of the inverse cumulative probability, the week case with 5 h per day of overgeneration as mean value is selected for the subsequent sizing of the energy storage and PEM-E systems. Such case is supposed to be a good trade-off between the storage/hydrogen capacity and the percentage of covered occurrences (equal to 67 % on a yearly base) as visible in Fig. 3.

Consequently, as cautionary hypothesis, among the 8 weeks characterized by 5 daily hours of OG, the OG power profile corresponding to the week with the minimum daily average power is selected. Such a week corresponds to the week #49 of the annual OG profile, characterized by peak and mean power values of 5.3 GW and 0.366 GW, respectively. Considering the power supply of all the 67 FCSs, such power values are greater of one order magnitude than the ones required by the FCS load. Hence, the design constraints for energy storage and electrolyzer sizing, described in Section 2.3, must allow the postponed use of the OG energy during all day, since OG is available for 5 h per day.

As regards hydrogen refueling, a typical profile is implemented in Fig. 4, assuming a hydrogen quantity stored in a truck tank of 52 kg at 600 bar, that is enough to power a 40-tons truck for around 440 miles [22,23]. Such profile is repeated varying the number of hydrogen trucks circulating along the highways each day of the considered week, in order to perform a sensitivity analysis on PEM-E sizing for trucks refueling.

The profile presented in Fig. 4 is subsequently implemented in Simulink environment, as concerns the third investigated scenario (i.e., cases 7–9 described in Section 2.3). Aiming to define the peak periods of hydrogen refueling at the considered FCS, the number of BEVs charged over the time is determined by dividing the load of Fig. 2 into classes referred to the number of vehicles. Assuming that a single 350 kW fast charging column can simultaneously charge two vehicles, classes from 0 (i.e., no vehicle is charged, power is null) to 10 vehicles (corresponding to 1750 kW as FCS load power) are defined. Dividing the weekly FCS load day by day, two different peaks of vehicles charges arise from Fig. 5, specifically at 7 a.m. and 1 p.m., respectively corresponding to 6 and 9 vehicles.

2.2. Dynamic modeling

In this section, the dynamic modeling of the FCS for the three investigated alternatives is illustrated. Specifically, Sections from 2.2.1 to 2.2.3 show FCS model integrating LIB, VRFB and LIB/PEM-E, respectively. The electrical architectures and Simulink models of the

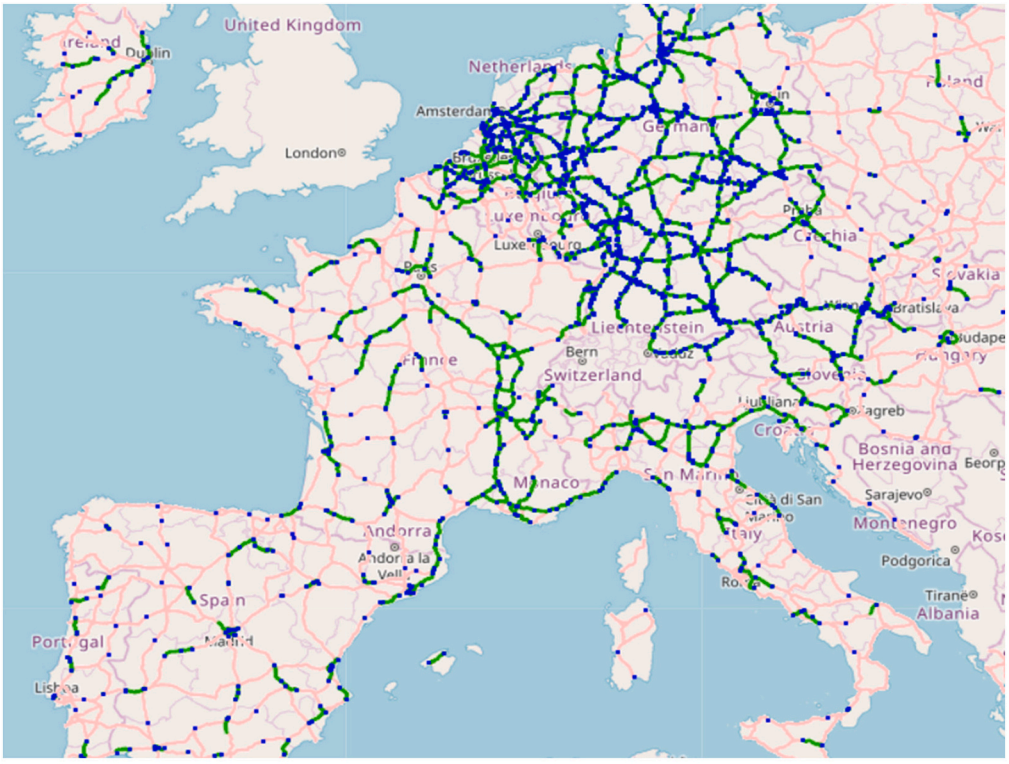

a)

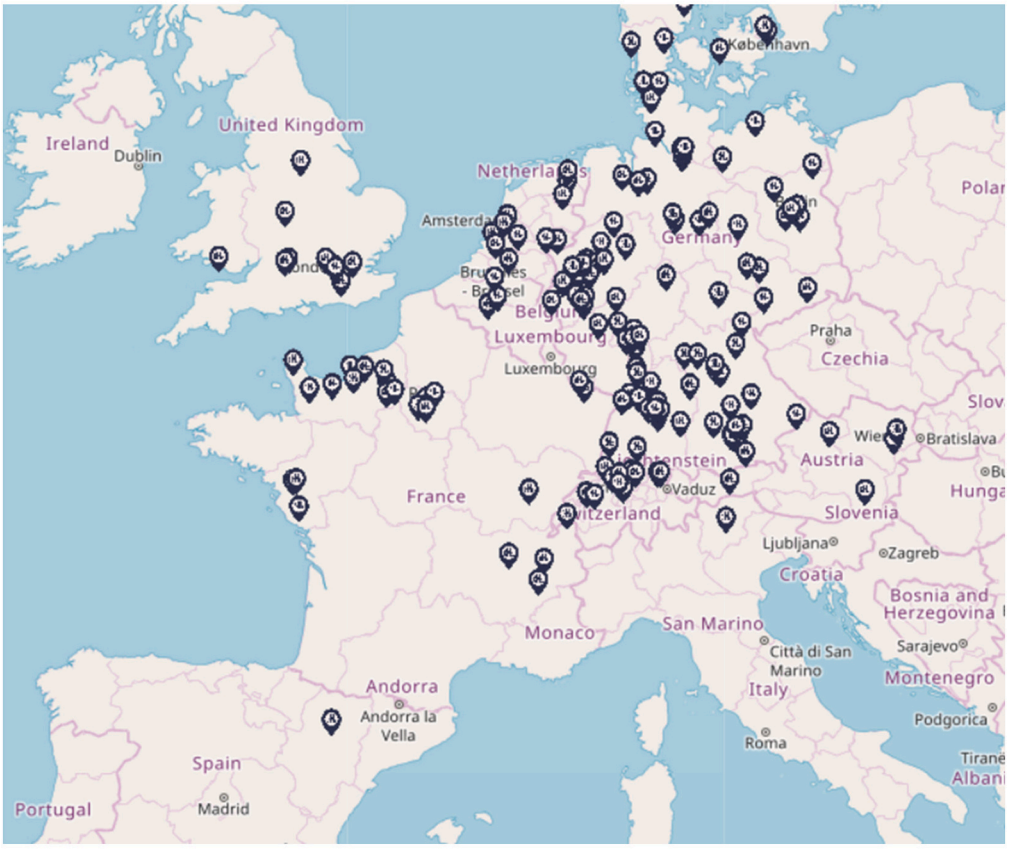

b)

Fig. 1. Current European infrastructure relating to a) fast charging of electric vehicles (blue points), highlighting the aspirational target of having a minimum coverage with public/semi-public e-charging points of minimum 150 kW power every 60 km and, b) hydrogen refueling stations [12,13]. (For interpretation of the references to colour in this figure legend, the reader is referred to the web version of this article.)

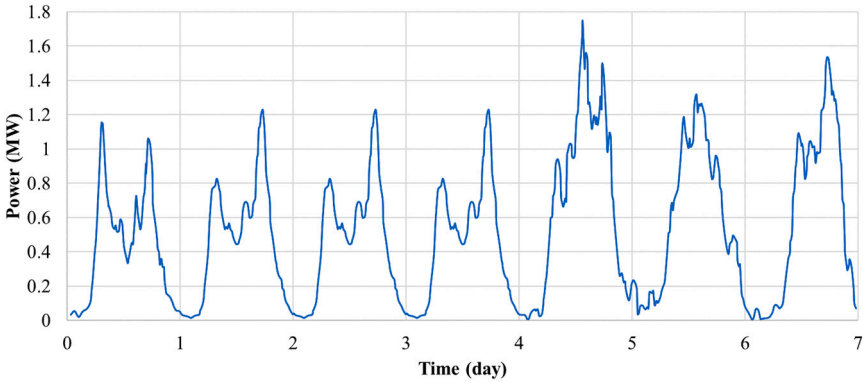

Fig. 2. Weekly trend of the considered FCS load, deduced from [21].

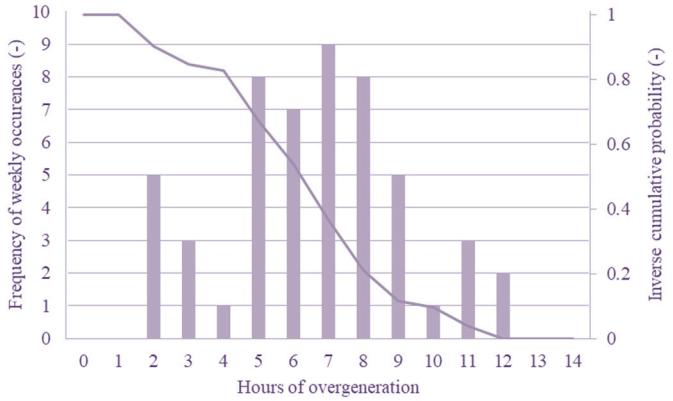

Fig. 3. Frequency of the occurrences and inverse cumulative probability, in reference to the average value of the daily hours of overgeneration during each week of the year.

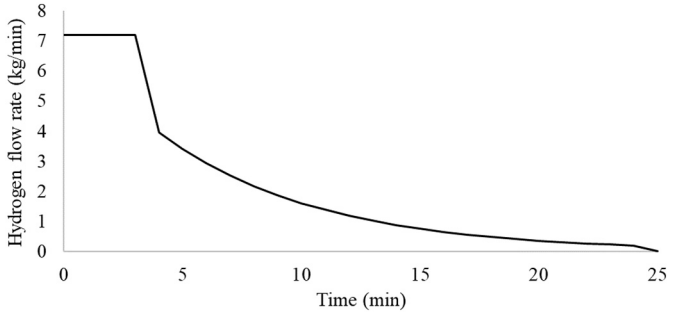

Fig. 4. Hydrogen mass flow rate over the time for a single truck refueling.

FCS are depicted in Fig. 6. In detail, the LIB/VRFB is connected to the common DC bus by means of a buck/boost converter and the PEM-E by means of a buck converter. The FCS load is considered a DC load according to the technical features of the installed recharging DC columns [24]. The developed Simulink dynamic models are shown in Fig. 6 b) and d) respectively for LIB/VRFB, and LIB-PEM-E. Specifically, in the orange section it is implemented the instantaneous power management strategy that receives as inputs the current overgeneration (OG, red section). When OG is not null, it supplies both FCS load and battery (light blue subsystem) charging, computed in the green section. Otherwise, FCS load is supplied primarily by the battery discharging and secondly by the grid. Battery C-rates and minimum SoC constraints are implemented in the algorithm. A fixed-step solver is chosen for simulations, with a sampling time of 1 s. All the details concerning the power

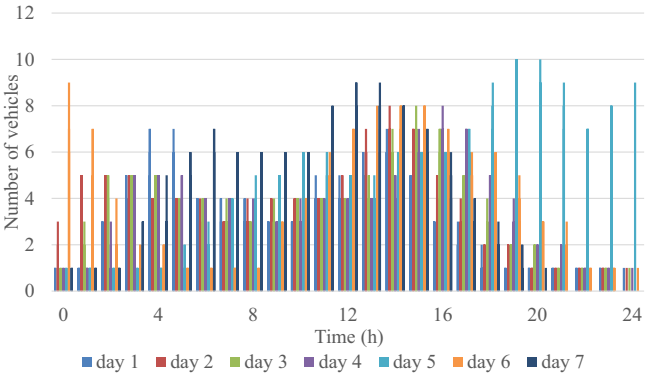

Fig. 5. Daily distribution of the electric vehicles' charges at FCS, according to the considered load profile.

management strategy are deeply illustrated in our previous study [25].

2.2.1. *FCS integrating Li-ion battery*

Battery performance and operating conditions are updated in real-time by the battery subsystem, depicted in Fig. 7. Specifically, it shows the dynamic modeling of Li-ion battery. Such model is developed by implementing open circuit voltage and internal resistance gathered data through look-up tables, according to the mathematical equations described in [26]. The model instantaneously updates the battery state of charge (SoC) according to current operating conditions and the battery measured technical features.

2.2.2. *FCS integrating VRFB*

As detailed in the previous Section 2.2.1, the developed VRFB model is based on the LIB one. However, the specific VRFB open circuit voltages and internal resistances during charge and discharge, measured by means of an experimental campaign at SoC variation, are implemented as reported in [27]. Fig. 8 depicts the VRFB model developed in Simulink environment.

2.2.3. *FCS integrating Li-ion battery and PEM electrolyzer*

To analyze a different scenario of FCS able to support both electric and hydrogen mobility, a PEM-E integrated to an FCS including a 10-MWh LIB is studied.

The model is developed implementing the polarization curve of a PEM-E, illustrated in [28], in a look-up table of Simulink environment, as shown in Fig. 9. In detail, green section represents the PEM-E implementation, while red and yellow sections highlight its activation and control, respectively. Concerning the activation, the electrolyzer starts to generate hydrogen when the OG reaches or overcomes the nominal power of the PEM-E stack to produce H_2 from renewable

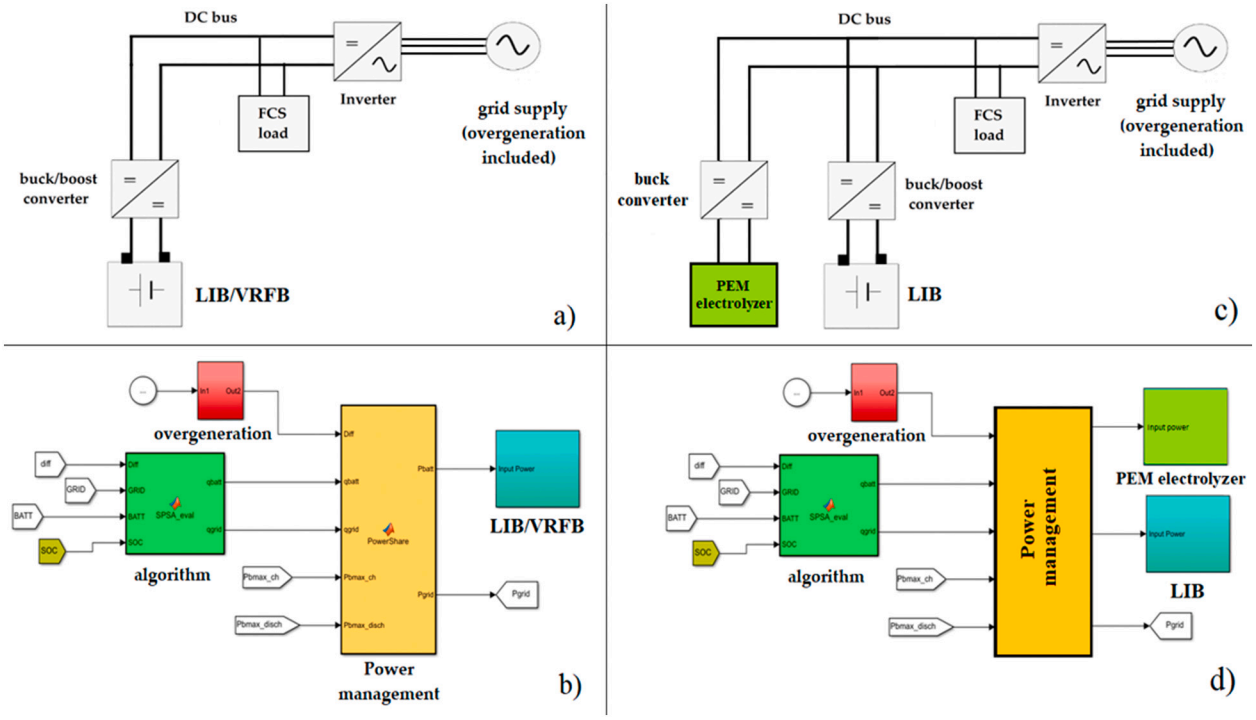

Fig. 6. Electrical architectures of the studied FCS for: a) LIB or VRFB, and c) LIB-PEM-E; dynamic models in MATLAB®/Simulink environment for: b) LIB or VRFB, and d) LIB-PEM-E.

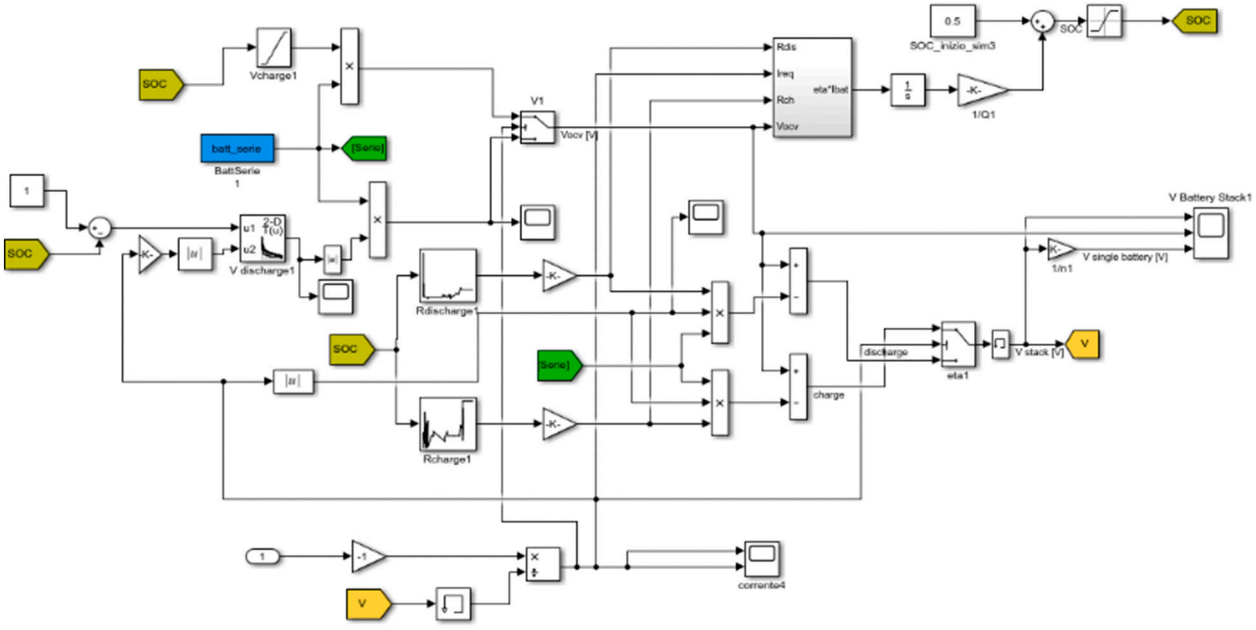

Fig. 7. Li-ion battery subsystem implementation.

sources. Instead, the control is performed instantaneously assessing the current amount of H_2 produced by the electrolyzer, consumed for refueling, and stored in the FCS tanks. An operating current density of 3 A cm^{-2} is imposed for the stack, according to literature specifications [29].

The produced instantaneous hydrogen molar flow rate ($q^r_{H_2}$), measured in kmol s^{-1}, is computed according to the following Eq. (1):

$$q^r_{H_2} = 2K_r I \tag{1}$$

where $K_r = \frac{N_0}{4F}$ is a modeling constant (in kmol $s^{-1}A^{-1}$) relating to the number of PEM-E cells in series (N_0) and the Faraday constant (F) in C $kmol^{-1}$, and I corresponds to the stack current (A).

Since the stack nominal voltage is imposed at 400 V, the cell area results to be 1024 cm^2 and the number of cells electrically in series is equal to 200. Therefore, the nominal power of each PEM-E stack is 1.25 MW (corresponding to a hydrogen production of about 20 kg h^{-1}). A round trip efficiency of 0.6 is considered for the PEM-E. Such values are in line with the specifications of Siemens Silyzer 200, as indicated in [30].

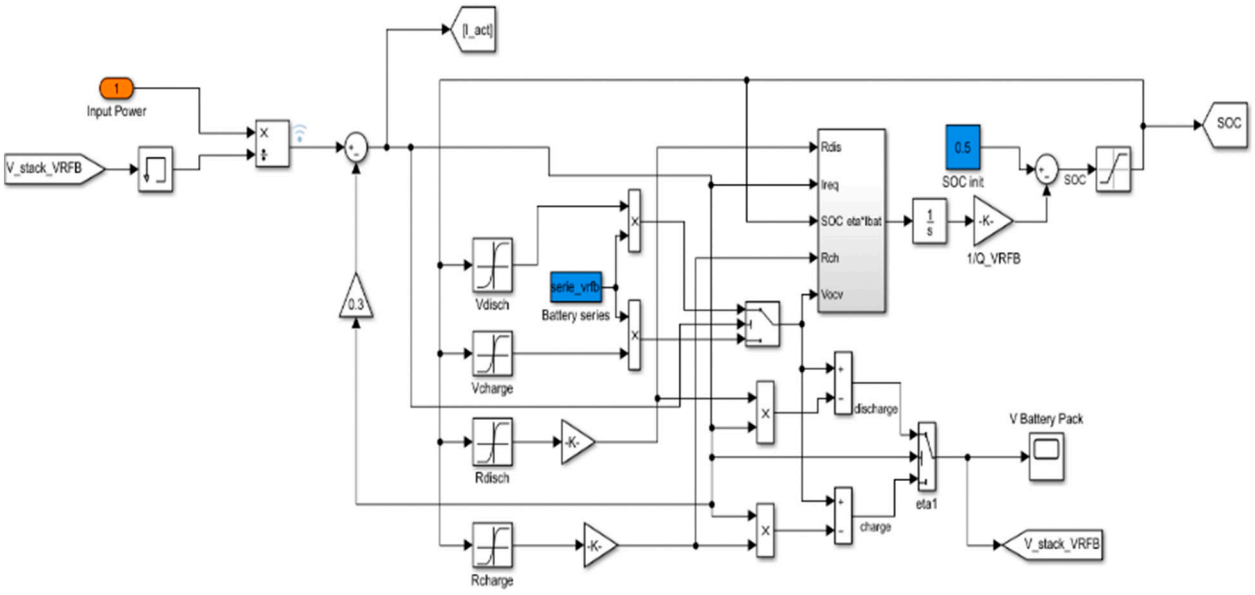

Fig. 8. Vanadium redox flow battery subsystem implementation.

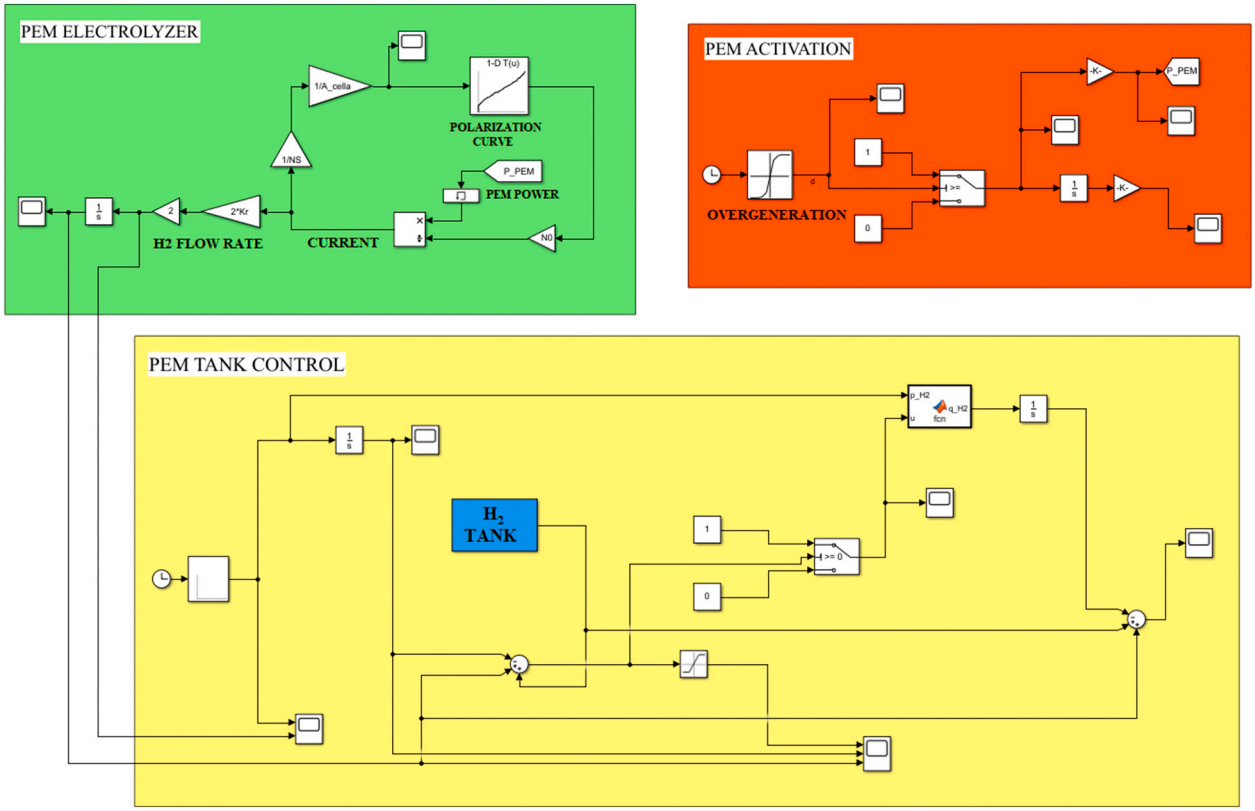

Fig. 9. PEM-E modeling. Green section represents the PEM-E, while red and green sections concern the activation and tank controls. (For interpretation of the references to colour in this figure legend, the reader is referred to the web version of this article.)

2.3. Simulation scenarios and component sizing

To define a proper sizing of the energy storage devices, different simulations are carried out in MATLAB®/Simulink environment varying the discharge/charge powers and the capacity of the considered battery. According to the statistical analysis described in Section 2.1, simulations are performed over a week. A maximum nominal capacity of 10 MWh is considered since it represents the mean daily amount of energy required by the FCS load during the hours of null OG. The sizing results for the three investigated technologies are shown in the following.

A. Li-Ion Battery and Vanadium redox flow battery

According to LIB specifications, three different simulation scenarios varying LIB power and capacity are defined, as listed in Table 1. The maximum C-rate for discharge and charge is fixed at C/2. A round trip

Table 1
Power and capacity values of the considered Li-ion battery packs.

Case	Nominal capacity (MWh)	Charge power (MW)	Discharge power (MW)
1	4	2	2
2	7	3.5	3.5
3	10	5	5

efficiency of 0.95 and a depth of discharge (DoD) of 90 % are considered.

Since VRFB can be independently sized in power and capacity, a different approach is followed. To this aim, fixing VRFB capacity at the values previously considered for LIB (i.e., 4, 7 and 10 MWh), a sensitivity analysis is performed reducing the VRFB charge and discharge maximum powers in reference to the values of Table 1. The purpose is to define the power values in the Cumulative Density Function (CDF) curve able to cover at least 90 % of occurrences over the considered week for the charge power and at least 95 % for the discharge power, respectively. It is highlighted that the determined charge/discharge powers are allowed for an operating current density range of 100–200 mA cm^{-2}, in line with commercial devices as indicated in [14]. A VRFB round trip efficiency of 0.72 and 100 % DoD are set. The resulting sizing data are listed in Table 2.

Fig. 10a reports the CDF curve relating to LIB and to VRFB power trends during discharge, while Fig. 10b depicts the CDF curve of the power supplied by the grid in case of OG absence. Specifically, it can be deduced from Fig. 10a how the considered energy storage systems operate at very low C-rates with respect to their capacity during discharging process. It is also emphasized that the amount of power required from the grid, when OG is null, is strongly reduced by the storage integration (see Fig. 10b).

As visible from Fig. 10b, in the 80 % of occurrences (i.e., CDF 80 %) the grid required power is lower than 450–650 kW, according to the installed storage capacity (see cases 1–6). These values are deeply reduced (−53 % for 10 MWh as storage capacity) if compared to the load power of 960 kW, corresponding to 80 % CDF in case of storage absence. This leads to a reduction of both required power and energy, emphasizing the benefits in terms of grid support introduced by battery integration into FCS.

B. PEM electrolyzer

As regards the PEM-E, the sizing is performed according to the required amount of hydrogen to be produced for refueling, in reference to the daily hydrogen trucks that drive along the highways. Since hydrogen infrastructure does not exist to date, a sensitivity analysis on the daily number of trucks is realized.

It is considered to have a PEM-E installed power of the same order magnitude of the LIB (10 MWh capacity and 5 MW dis-/charge power as in case 3 of Table 1). Moving from the FCS weekly profile, a statistical evaluation of the charging distribution over the time is carried out to find the peak hours for fast charging. Assuming that the hydrogen trucks are refueled at such hours, three different weekly profiles of H_2 refueling are generated, corresponding to:

i) two refuels per day, one starting at 7 a.m. and one at 1 p.m.,

Table 2
Sizing of the VRFB system for the three considered cases.

Case	Nominal capacity (MWh)	Battery nominal power @ 100 mA cm^{-2} (MW)	Max charge power (MW)	Max discharge power (MW)	Current density range (mA cm^{-2})
4	4	1	1.5	1.3	100–200
5	7	1.4	2	1.4	
6	10	1.4	2.5	1.4	

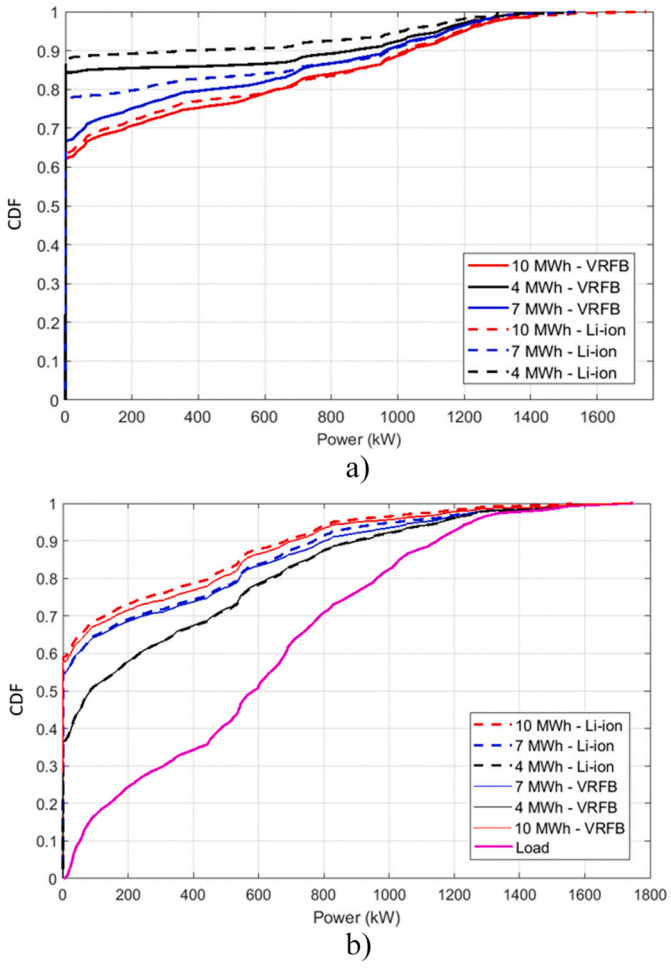

Fig. 10. CDF curve of: a) the mean discharge power of the LIB and VRFB; b) the grid mean power in case of OG absence, for the three considered installed capacities.

ii) four refuels per day, two starting at 7 a.m. and two at 1 p.m.,
iii) ten refuels per day, four starting at 7 a.m. and six at 1 p.m.

In reference to each scenario, PEM-E installed power is sized to reach the required hydrogen generation varying the number of stacks. Moreover, concerning the capacity of H_2 tanks, weekly simulations are run to define the minimum H_2 tank capacity needed for covering all the refueling, considering an initial level equal to 50 % of the maximum one. Capacity sizing is done also considering that one third of the weekly hydrogen requirement is externally provided by H_2 cylinder packs. Thus, the resulting power/capacity sizing of the PEM-E is listed in Table 3, taking into account that the produced hydrogen is stored in FCS tanks at a pressure of 350 bar.

3. Simulation results

In this section, the performed simulations to assess LIB, VRFB and LIB-PEM-E energy performances on the FCS are illustrated.

A. FCS integrating Li-ion Battery

The trends of the most significant parameters during the simulations are illustrated in the following Figs. 11–13. Specifically, the red trend represents the renewable power due to overgeneration (OG); when available, it supplies both FCS load (dashed black profile) and battery producing its charging (SoC profile is highlighted by the dashed blue

Table 3
Sizing of the PEM-E electrolyzer-LIB integration into FCS for the three different H_2 refueling profiles considered.

Case	Li-ion Battery			PEM electrolyzer			
	Nominal capacity (MWh)	Charge power (MW)	Discharge power (MW)	H_2 capacity (kg)	H_2 volume (at 350 bar) (m^3)	Nominal power (MW)	Stack number
7	10	5	5	300	13.3	1.25	1
8	10	5	5	631	28	2.5	2
9	10	5	5	1660	73.8	6.25	5

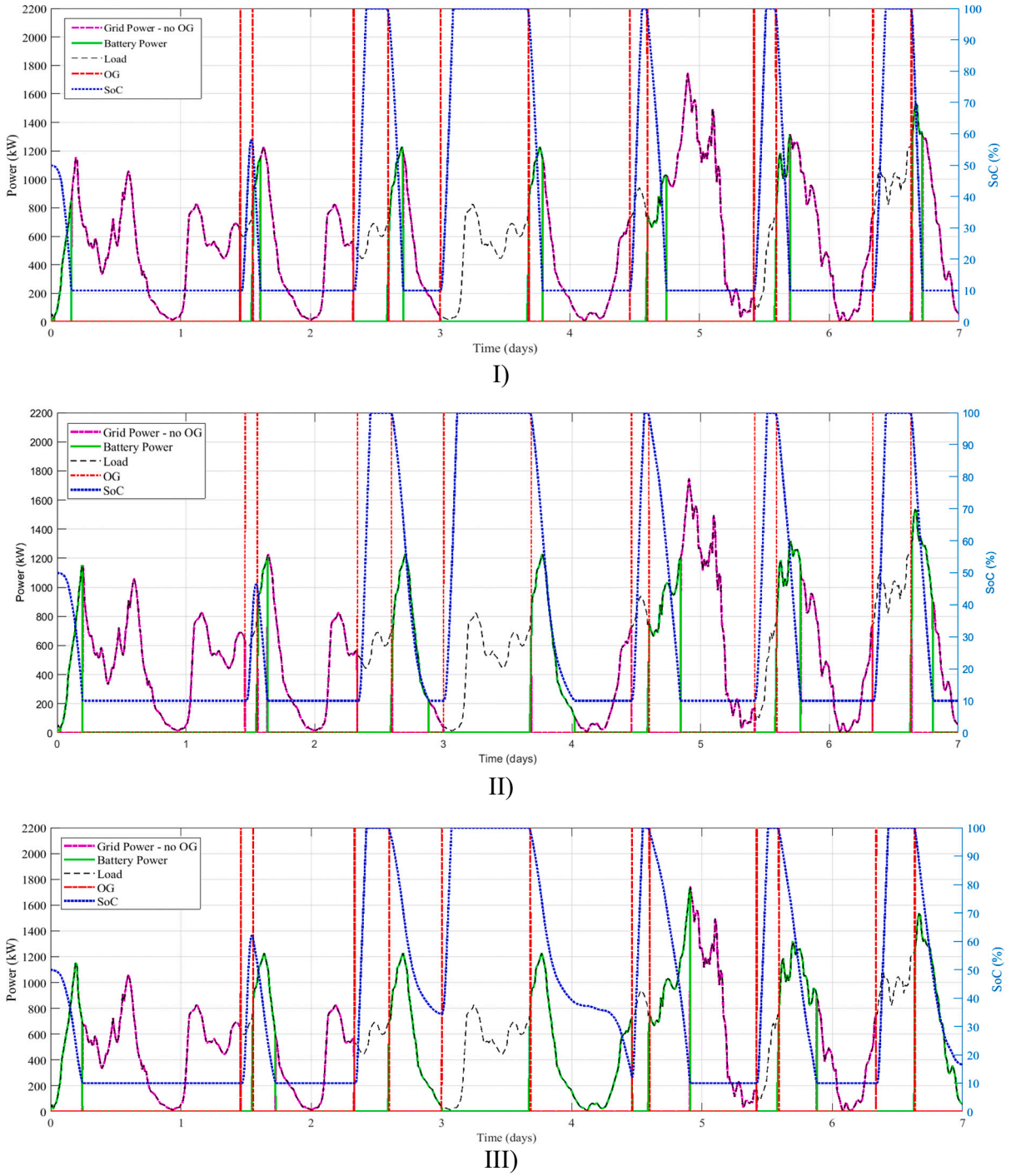

Fig. 11. Trends of the main parameters for FCS integrating LIB. Grid power exchanges is represented by dashed pink line, battery power trend by green line, the FCS load in dashed black, OG in dashed red and battery SoC in dashed blue line. Specifically, I) refers to 4-MWh LIB, II) to 7-MWh LIB and III) to 10-MWh LIB. (For interpretation of the references to colour in this figure legend, the reader is referred to the web version of this article.)

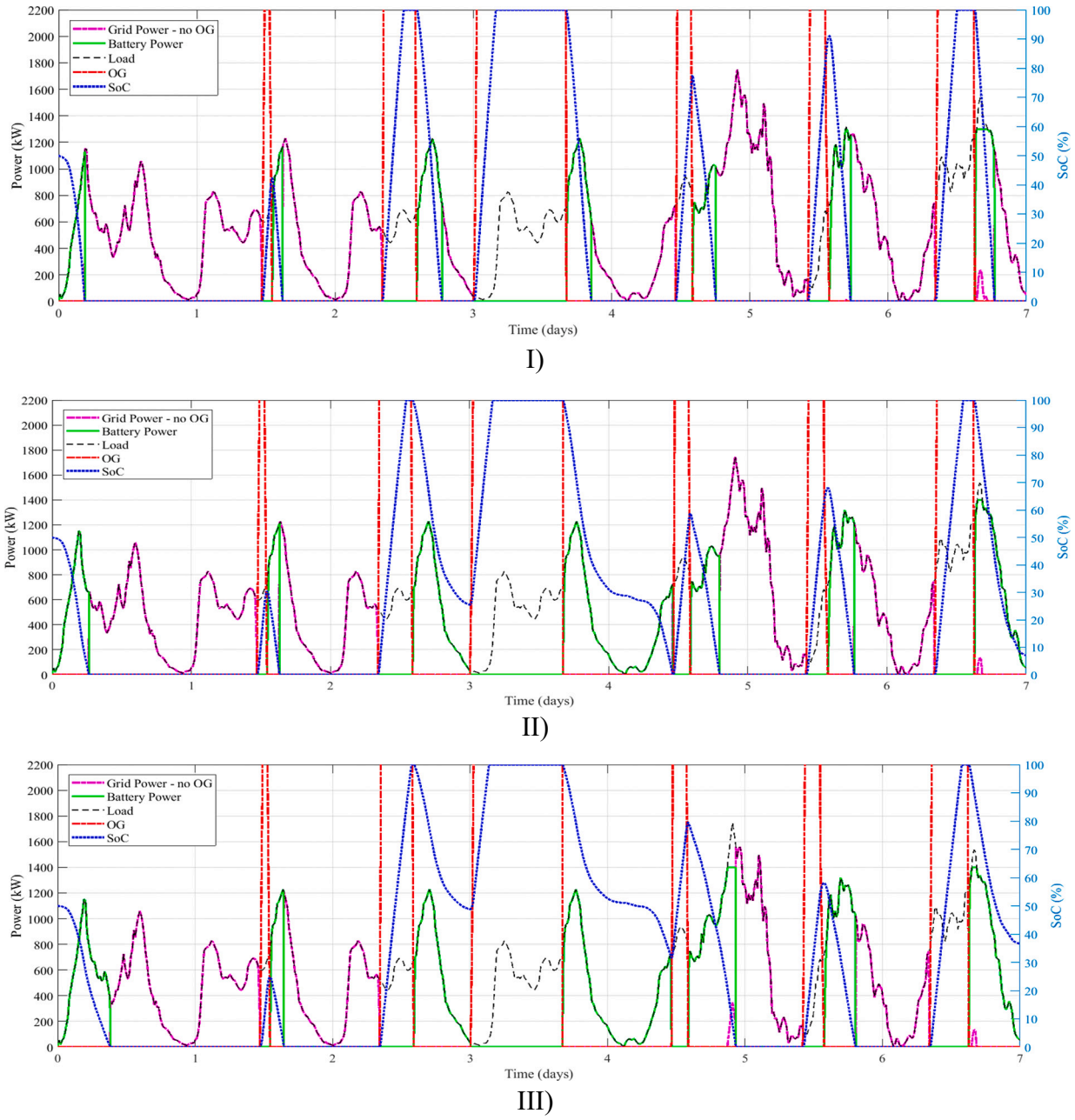

Fig. 12. Trends of the main parameters for FCS integrating VRFB. Grid power exchanges is represented by dashed pink line, battery power trend by green line, the FCS load in dashed black, OG in dashed red and battery SoC in dashed blue line. Specifically, I) refers to 4-MWh VRFB, II) to 7-MWh VRFB and III) to 10-MWh VRFB. (For interpretation of the references to colour in this figure legend, the reader is referred to the web version of this article.)

line). On the other hand, when the OG is null the FCS load is supplied by the battery (the green trend represents the discharge battery power) until its SoC reaches the minimum threshold, set at 10 %. Finally, when LIB is discharged, the FCS load is provided by the grid (P_{grid}, pink dashed line).

B. FCS integrating Vanadium redox flow battery

Fig. 12 depicts the evolution of the simulated parameters for the FCS integrating VRFB, varying the capacity/powers according to the cases listed in Table 2. The same considerations for LIB can be done for VRFB, except for the SoC that can reach 0 %, since VRFB can operate at 100 % DoD without negative effects on lifespan, according to [27].

C. FCS integrating Li-ion battery / PEM electrolyzer

As regards the integration of LIB/PEM-E into the FCS, allowing both fast charging recharge and hydrogen refueling, simulation results are illustrated in Fig. 13. In detail, Fig. 13a represents the FCS hydrogen refueling over the considered week, while Fig. 13b the evolution of consumed/generated hydrogen stored in the H_2 pressurized tanks and in the external cylinder packs. Graphs a) in Fig. 13 depict the vehicles hydrogen refueling during the days of the considered week (2, 4 and 10 refueling occurrences per day for cases 7,8 and 9 respectively), referring to the mass flow rate illustrated in Fig. 4. It can be seen from the graphs b) in Fig. 13 that the hydrogen stored in the tank is completely consumed in about two days, since the OG in the first two days of the week is very low. In particular, for case 9 (5 PEM-E modules) no hydrogen is locally produced in the first two days due to the lower instantaneous OG power in relation to the installed PEM-E power. Moreover, graphs c) and d) of Fig. 13 report the locally produced hydrogen flow rate and the absorbed

power from electrolyzer system over the considered week, respectively.

Concerning the 10-MWh Li-ion battery for cases 7–9, Fig. 14 illustrates the parameters of interest, as already depicted in the previous paragraph for LIB and VRFB (cases 1–6). It is emphasized that Fig. 14 depicts only one of the three simulated scenarios (i.e., cases 7–9) since there are no relevant differences among them.

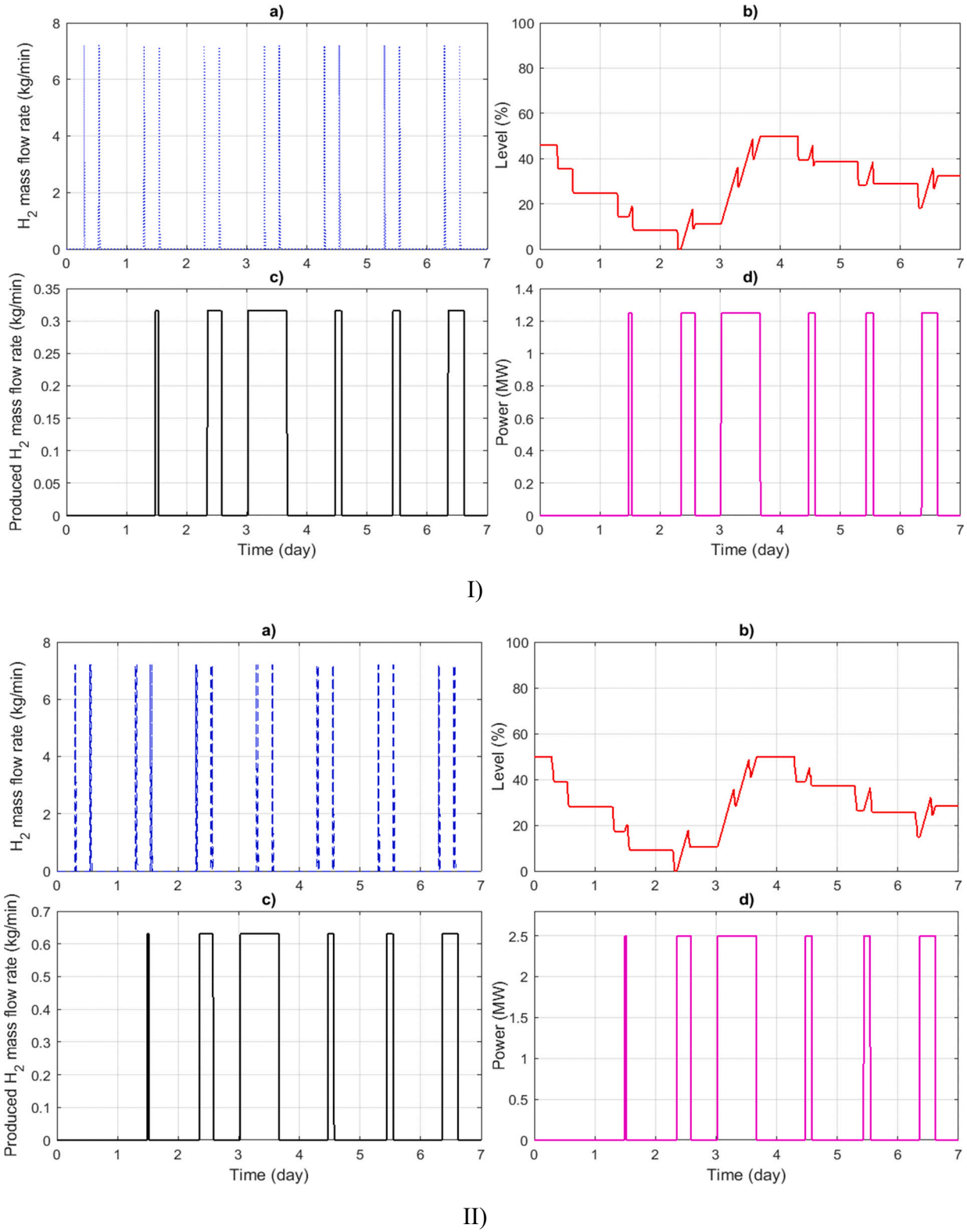

Fig. 13. Main results of simulations concerning FCS integrating PEM-E. Specifically, a) represents the H_2 refueling mass flow rate, b) the hydrogen consumption (tank plus cylinder packs), c) is the generated hydrogen mass flow rate and d) the amount of required power of the PEM-E. I), II) and III) are referred to the case 7 (i.e., 1 PEM-E module), case 8 (i.e., 2 PEM-E modules) and case 9 (i.e., 5 PEM modules), respectively.

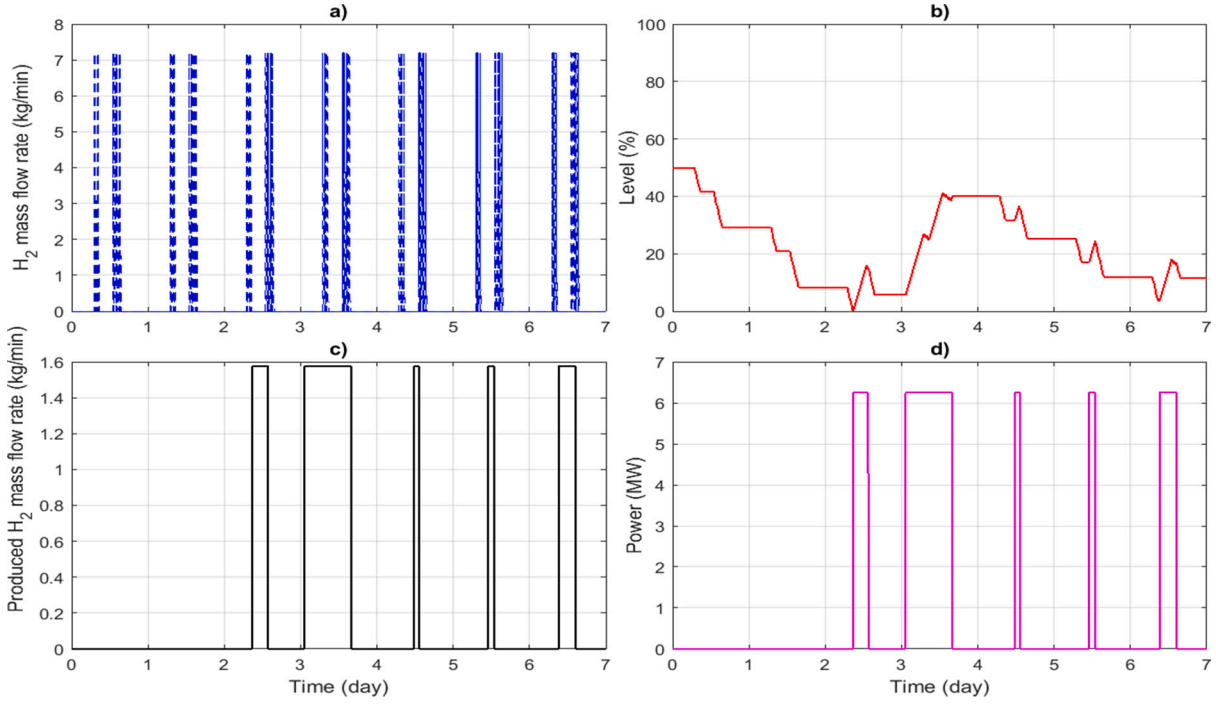

III)

Fig. 13. (*continued*).

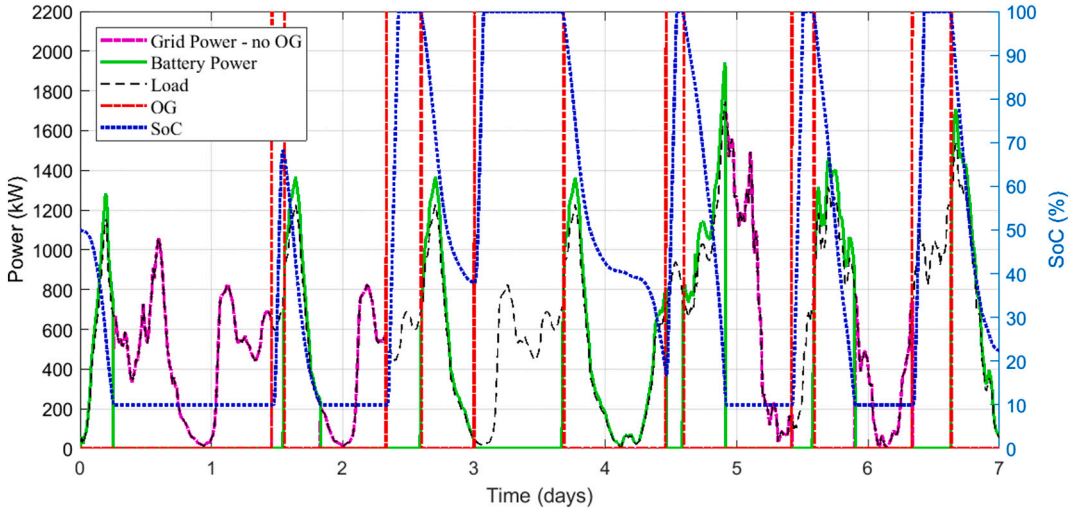

Fig. 14. Trends of the main parameters of the FCS integrating LIB and PEM-E (case 7). Grid power exchanges is represented by dashed pink line, battery power trend by green line, the FCS load in dashed black, OG in dashed red and battery SoC in dashed blue line. (For interpretation of the references to colour in this figure legend, the reader is referred to the web version of this article.)

Table 4
Summary of energy storage and hydrogen technologies integration into the considered FCS.

Case	Energy from grid (kWh/week)	Energy from OG (kWh/week)	FCS electric requirements (kWh/week)	Charging/H_2 refueling from OG (%)
1 - LIB	57,024	41,424	98,448	42 %
2 - LIB	43,572	54,876		56 %
3 - LIB	33,200	65,248		66 %
4 - VRFB	51,053	47,395		48 %
5 - VRFB	39,606	58,842		60 %
6 - VRFB	32,501	65,947		67 %
7 - LIB/PEM-E	33,147	65,301		66/66 %
8 - LIB/PEM-E	33,733	64,715		66/66 %
9 - LIB/PEM-E	34,703	63,745		65/66 %

Table 4 reassumes the data of the resulting energy performances in reference to the investigated FCS scenarios. Specifically, the amount of energy provided by the grid in case of OG absence, the energy covered by OG and the load requirement are listed below, together with the percentage of renewable OG exploitation to satisfy the FCS load. Moreover, as regards cases 7–9, the percentage of OG exploitation is referred to the energy required by PEM-E for hydrogen generation. Although the hydrogen production into FCS is totally powered by OG, it is highlighted that one third of hydrogen is externally provided through cylinder packs. Thus, the local hydrogen production for refueling corresponds to about 66 % of the total stored hydrogen into FCS.

4. Analysis of the energy storage and hydrogen integration into FCS

To assess the feasibility of energy storage/hydrogen integration into FCSs, a detailed analysis on the encumbrance of the alternatives is carried out. Results for all the studied scenarios for FCS are listed in Table 5. In order to define the encumbrance of each system, the volumetric factor K, expressed in m^3 MW, is defined in reference to the maximum installed power (i.e., the maximum charging power for LIB and VRFB, and the nominal power for PEM-E). Specifically, concerning LIBs, K factor is determined moving from the specifications of a 9.6 MW/3.8 MWh LIB rack of $16.2 \times 2.6 \times 2.9$ m^3 dimensions, as detailed in [31]. According to such specifications, the total volume of the LIB rack is computed by means of linear interpolation since the capacities are in the same capacity range. Hence, a 4 MWh LIB has a volume equal to about 128 m^3, as reported in Table 5. Therefore, dividing the LIB rack total volume for its maximum power, a K factor of about 64 m^3/MW is determined for LIBs (i.e., cases 1–3 and 7–9). On the other hand, VRFB and PEM-E encumbrances are computed according to their specifications, indicated in [30,32] respectively. All data, including the total volume, needed for factor K calculation are reported in Table 5. It is emphasized that the volumetric factor relative to PEM-E is only referred to the stack (i.e., Silyzer 200), as other PEM-E components, listed in the following, are separately considered (see Table 5) and properly scaled according to PEM-E powers:

- The water treatment system, that removes toxic compounds eventually present in the water. This system has an encumbrance of 42 m^3 for the single considered stack.
- The cooling system, which has a volume of 52.5 m^3 per stack.
- The deoxo dryer, that is used to remove any percentage of water from the produced hydrogen. Its volume corresponds to 15.75 m^3.
- The chiller, which volume is equal to 15.75 m^3.

Moreover, the hydrogen is stored in the FCS tank at 350 bar, and one third of the necessary hydrogen is provided by means of external cylinder packs at the same pressure. The hydrogen density at 350 bar is of 22.5 kg m^{-3}.

From Table 5 it can be deduced that the worst case for encumbrances is represented by case 6, corresponding to the 10-MWh VRFB, due to its low energy density (20–30 Wh kg^{-1}) with respect to LIB (more than 250 Wh kg^{-1}). To compare the alternatives for FCS, three indexes are defined, as described in Eqs. (2)–(4):

$$K_{BEV} = \frac{\text{average number of charged BEVs per day}}{\text{Total volume } (m^3)} \quad (2)$$

$$K_{FCEV} = \frac{\text{average number of refueled FCEVs per day}}{\text{Total volume } (m^3)} \quad (3)$$

$$E_v = \frac{\text{charged/refueled energy per day (kWh)}}{\text{Total volume } (m^3)} \quad (4)$$

where the total volume (see Table 5) represents the corresponding volume of the storage/hydrogen devices, relating to the investigated cases. Furthermore, to perform a comparison between the number of hydrogen trucks refueled and BEVs charged, the daily average number of charged/refueled vehicles is computed considering the percentage of charging/refueling made by exploiting the renewable OG, according to Table 4. As regards BEVs, it is considered 50-kWh as mean capacity value of the battery installed on-board, and of 52 kg for truck hydrogen tank capacity. The truck tank capacity corresponds approximately to 10 FCEVs (with a tank of more than 5 kg), as indicated in [33]. Therefore, such FCS integrating hydrogen generation can refuel 20, 40 and 100 FCEVs per day, respectively in reference to cases 7, 8 and 9.

Such comparison in terms of both the average daily number of charged/refueled vehicles and the charged/refueled energy per volume is detailed in Table 6. It is highlighted that, comparing K_{EV} and K_{FCEV}, the number of vehicles charged/refueled per occupied cube meter in the case of PEM-E integration is about of one order magnitude lower than LIB (cases 7-8-9). Very low values of K_{EV} are registered for VRFB, since the electrolyte has a very low energy density with respect to LIBs. Furthermore, to have a more comprehensive overview, a comparison related to the charged/refueled kWh over the volume occupied by the storage section (E_v) is realized. Specifically, Fig. 15 illustrates the charged/refueled energy (kWh) per m^3 of the system encumbrance in all the simulated scenarios. Because of the low energy density (i.e. 20–30 Wh kg^{-1}), VRFB represents the worst solution in terms of the number of charged vehicles in relation to the required volume for its installation. Anyway, VRFB features as the independent power and capacity sizing, high lifespan and no hysteresis represent a valuable alternative for custom applications. On the other hand, taking into account the high specific energy density of hydrogen (i.e. 33.33 kWh kg^{-1}), the gap between PEM-E and LIB, in terms of E_v index, is significantly reduced with respect to the K_{FCEV} vs. K_{BEV} factors. Specifically, such gap passes from about 0.067 vs. 0.57 vehicles per m^3 to 11.7 vs. 28 kWh m^{-3}.

Table 5
Volumetric encumbrances of the energy storage and hydrogen electrolyzer for each investigated scenario.

Case	Max power (MW)	Rack height (m)	Rack area (m^2)	Volumetric factor K (m^3/MW)	H_2 tank volume (m^3)	External hydrogen cylinder pack (m^3)	PEM-E other components (m^3)	Total volume (m^3)
1	2	2.91	44.1	64.2	–	–	–	128.4
2	3.5	2.91	77.2		–	–	–	224.7
3	5	2.91	110.3		–	–	–	321.1
4	1.5	7.5	119.6	597.8	–	–	–	896.7
5	2	7.5	209.2	784.6	–	–	–	1569.2
6	2.5	7.5	298.6	896.7	–	–	–	2241.8
7 (LIB/PEM-E)	5/1.25	2.91/3	110.3/68.3	64.2/46.9	13.3	6.9	126	321/204.8
8 (LIB/PEM-E)	5/2.5		110.3/137.2		28	14.4	252	321/411.6
9 (LIB/PEM-E)	5/6.25		110.3/345		73.8	38	630	321/1035

Table 6
Encumbrances of the alternatives for the studied scenarios.

Case	FCS storage	Battery/PEM-E max power (MW)	Average number of BEVs charged per day	FCEVs refueled per day	K_{BEV} (BEVs per m^3)	K_{FCEV} (FCEVs per m^3)	E_v (kWh m^{-3})
1	LIB	2	118	–	0.92	–	46.0
2	LIB	3.5	157	–	0.70	–	35.0
3	LIB	5	185	–	0.58	–	28.9
4	VRFB	1.5	135	–	0.15	–	7.5
5	VRFB	2	169	–	0.11	–	5.4
6	VRFB	2.5	188	–	0.08	–	4.2
7	LIB/PEM-E	5/1.25	186	13	0.58	0.0674	29.0/11.7
8	LIB/PEM-E	5/2.5	185	27	0.58	0.0671	28.8/11.6
9	LIB/PEM-E	5/6.25	182	67	0.57	0.0669	28.3/11.6

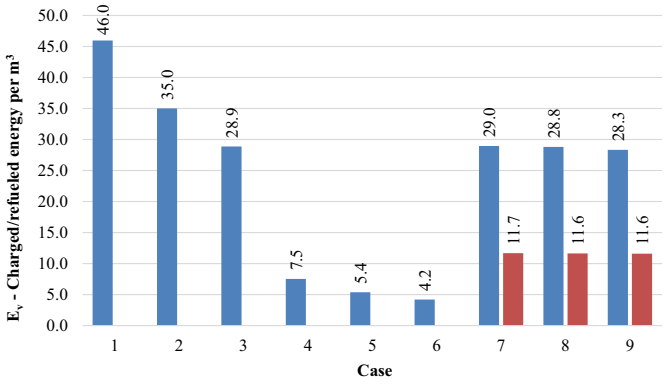

Fig. 15. Encumbrances in terms of charged/refueled energy per volume of installed system for the studied scenarios. Specifically, blue bars indicate the fast charging for BEVs, red bars the hydrogen refueling for FCEVs. (For interpretation of the references to colour in this figure legend, the reader is referred to the web version of this article.)

5. Conclusions

Fast-charging stations along the highways and hydrogen refueling represent a key factor to allow the electric mobility transition. This research study illustrates three different alternatives of energy storage integration into FCSs aiming to support BEV fast charging and FCEV refueling by exploiting the surplus of renewable energy estimated at 2040 by Terna S.p.A.. Moreover, in the third scenario, a PEM electrolyzer is also considered, coupled to a Li-ion battery section, to assess the feasibility of local hydrogen generation into FCS in the view of FCEVs spread. The integration of the alternatives into the FCS is evaluated based on volumetric encumbrance per charged/refueled vehicle.

The main outcomes highlight that the PEM-E occupied volume per vehicle is about of one order magnitude greater than LIB (cases 7-8-9). On the other hand, if the three scenarios are compared in terms to the charged/refueled kWh per occupied volume (E_v), the difference between PEM-E and LIB is significantly reduced (i.e., 11.7 vs. 28 kWh m^{-3}). Anyway, BEVs fast charging thorough highways FCSs integrating LIBs exhibits in terms of volume and territory occupation a charging capacity more than twice with respect to hydrogen refueling with on-site H_2 production.

Moreover, the required power from the grid reduces up to −53 % for the 10 MWh LIB if compared to the load power in case of storage absence. This emphasizes the benefits in terms of grid support introduced by battery integration into FCSs allowing the respect of the transport constraints, reducing under voltage and power stability issues as well. Finally, once the FCS configuration here proposed is implemented at the systemic level, the operation of the energy storage sections could be optimized also to provide services to the grid with further benefits.

CRediT authorship contribution statement

Conceptualization, L.B. and D.Z.; methodology, D.P.; software, D.P.; validation, D.P., M.L., G.B. and L.B.; formal analysis, D.P.; investigation, D.P.; writing - original draft preparation, D.P.; writing - review and editing, G.B., D.Z. and L.B.; visualization, D.P.; supervision, G.B., L.B; project administration, L.B.; funding acquisition, L.B.

Declaration of competing interest

The authors declare that they have no known competing financial interests or personal relationships that could have appeared to influence the work reported in this paper.

Data availability

The data that has been used is confidential.

Acknowledgment

Authors acknowledge the support of the European Commission under the project STORIES (GAP-101036910). Also project LIFE3H (LIFE 20 ENV/IT/000575) is acknowledged. Terna S.p.A. is acknowledged for providing overgeneration data at 2040.

References

[1] IEA, Global energy-related CO2 emissions by sector [Online]. Available: https://www.iea.org/data-and-statistics/charts/global-energy-related-co2-emissions-by-sector [Accessed: 26-May-2022].
[2] European Commission, 2050 long-term strategy | Climate Action [Online]. Available: https://ec.europa.eu/clima/policies/strategies/2050_en, 2017 [Accessed: 17-May-2021].
[3] H.S. Das, M.M. Rahman, S. Li, C.W. Tan, Electric vehicles standards, charging infrastructure, and impact on grid integration: a technological review, Renew. Sust. Energ. Rev. 120 (2020), 109618.
[4] M. Brenna, F. Foiadelli, C. Leone, M. Longo, Electric vehicles charging technology review and optimal size estimation, J. Electr. Eng. Technol. 15 (3) (2020) 2539–2552.
[5] P. Wolfram, N. Lutsey, Electric vehicles: Literature review of technology costs and carbon emissions, in: The International Council on Clean …, 2016, pp. 1–23, no. July.
[6] C. Suarez, W. Martinez, Fast and ultra-fast charging for battery electric vehicles - a review, in: 2019 IEEE Energy Conversion Congress and Exposition, ECCE 2019, 2019, pp. 569–575.
[7] Statista, Renewable power generation share worldwide [Online]. Available: https://www.statista.com/statistics/489131/share-of-renewables-in-power-generation-globally/, 2021 [Accessed: 27-May-2022].
[8] Eni, "How to make the use of hydrogen for transportation possible?" [Online]. Available: https://www.eni.com/en-IT/sustainable-mobility/hydrogen-transports.html. [Accessed: 27-May-2022].
[9] European Commission, The EU's hydrogen strategy and its geopolitical challenges [Online]. Available: https://www.ispionline.it/en/pubblicazione/eus-hydrogen-strategy-and-its-geopolitical-challenges-30521, 2020 [Accessed: 27-May-2022].

[10] M. Dotzauer, K. Oehmichen, D. Thrän, C. Weber, Empirical greenhouse gas assessment for flexible bioenergy in interaction with the German power sector, Renew. Energy 181 (Jan. 2022) 1100–1109.
[11] P. Chakraborty, R. Parker, T. Hoque, J. Cruz, L. Du, S. Wang, S. Bhunia, Addressing the range anxiety of battery electric vehicles with charging en route, Scientific Reports 12 (1) (2022) 1–15.
[12] "Idrogeno". [Online]. Available: https://www.autobrennero.it/it/sostenibilita/idrogeno/. [Accessed: 27-May-2022].
[13] EU Commission, "TENtec Interactive Map Viewer." [Online]. Available: https://ec.europa.eu/transport/infrastructure/tentec/tentec-portal/map/maps.html. [Accessed: 27-May-2022].
[14] A. Mourad, M. Hennebel, A. Amrani, A.Ben Hamida, Deploying fast-charging stations for electric vehicles based on mobility flows and local photovoltaic production, in: International Conference on the European Energy Market 2020, EEM, 2020. September.
[15] S.A. Funke, P. Plötz, A Techno-economic Analysis of Fast Charging Needs in Germany for Different Ranges of Battery Electric Vehicles, 2017.
[16] S. LaMonaca, L. Ryan, The state of play in electric vehicle charging services – a review of infrastructure provision, players, and policies, Renew. Sust. Energ. Rev. 154 (Feb. 2022), 111733.
[17] M. Wang, X. Dong, Y. Zhai, Optimal Configuration of the Integrated Charging Station for PV and Hydrogen Storage, 2021.
[18] D. Li, A. Zouma, J.T. Liao, H.T. Yang, An energy management strategy with renewable energy and energy storage system for a large electric vehicle charging station, eTransportation 6 (Nov. 2020).
[19] M. Shafiei, A. Ghasemi-Marzbali, Fast-charging station for electric vehicles, challenges andissues: a comprehensive review, Journal of Energy Storage 49 (2022).
[20] "Colonnine in autostrada, ci siamo: Aspi apre le prime ultra fast". [Online]. Available: https://insideevs.it/news/506831/colonnine-autostrada-piano-aspi-hpc/. [Accessed: 29-Oct-2021].
[21] P. Jochem, E. Szimba, M. Reuter-Oppermann, How many fast-charging stations do we need along European highways? Transp. Res. Part D: Transp. Environ. 73 (January) (2019) 120–129.
[22] "Under the skin: The logic behind Bosch's plans for hydrogen fuel cell trucks | Autocar". [Online]. Available: https://www.autocar.co.uk/car-news/technology-news/under-skin-logic-behind-boschs-plans-hydrogen-fuel-cell-trucks. [Accessed: 23-May-2022].
[23] M. Deymi-Dashtebayaz, M. Farzaneh-Gord, N. Nooralipoor, H. Niazmand, The complete modelling of the filling process of hydrogen onboard vehicle cylinders, Braz. J. Chem. Eng. 33 (2) (2016) 391–399.
[24] "In autostrada si ricarica l'auto elettrica, colonnine ogni 50 km (mappa)." [Online]. Available: https://www.newsauto.it/notizie/autostrada-ricarica-auto-elettrica-dc-veloce-fast-aree-di-servizio-colonnine-mappa-2020-251568/#foto-2. [Accessed: 17-Nov-2021].
[25] D. Pelosi, A. Baldinelli, G. Cinti, D.A. Ciupageanu, P.A. Ottaviano, F. Santori, F. Carere, L. Barelli, Battery-hydrogen vs. flywheel-battery hybrid storage systems for renewable energy integration in mini-grid: a techno-economic comparison, Journal of Energy Storage 63 (2023) 106968. March.
[26] L. Barelli, G. Bidini, F. Bonucci, L. Castellini, S. Castellini, P.A. Ottaviano, D. Pelosi, A. Zuccari, Dynamic analysis of a hybrid energy storage system (H-ESS) coupled to a photovoltaic (PV) plant, Energies 11 (2) (2018).
[27] L. Barelli, G. Bidini, P.A. Ottaviano, D. Pelosi, Vanadium redox flow batteries application to electric buses propulsion: Performance analysis of hybrid energy storage system, Journal of Energy Storage 24 (2019) 100770. February.
[28] Davidlfritz, "PEM electrolysis loss breakdown," Wikipedia [Online]. Available: https://en.wikipedia.org/wiki/File:PEM_electrolysis_loss_breakdown.pdf, 2013 [Accessed: 23-May-2022].
[29] S.A. Grigoriev, V.N. Fateev, D.G. Bessarabov, P. Millet, Current status, research trends, and challenges in water electrolysis science and technology, Int. J. Hydrog. Energy 45 (49) (2020) 26036–26058.
[30] Siemens Energy, Overview of the PEM Silyzer family, 2020.
[31] L. Barelli, G. Bidini, P.A. Ottaviano, D. Pelosi, M. Perla, F. Gallorini, M. Serangeli, A novel concept for grid Li-ion BESS safety: integration of vanadium-air flow battery technology in fire protection system, J. Energy Storage 42 (Oct. 2021), 103086.
[32] Cellcube, Datasheet FB250/FB500 Series Release 4.00 [Online]. Available: https://www.cellcube.com/wp-content/uploads/2021/08/Cellcube_Datenblatt_allgemein_en_01.pdf [Accessed: 27-May-2022].
[33] Toyota, Toyota Mirai Specs & Options [Online]. Available: ttps://www.toyota.com/mirai/features/mpg_other_price/3002/3003, 2022 [Accessed: 26-May-2022].